

Article

Impact of Using Tungsten, Cobalt, and Aluminum Additives on the Tribological and Mechanical Properties of Iron Composites

Moustafa M. Mohammed ¹, Nashmi H. Alrasheedi ², Omayma A. El-Kady ³, Joy Djuansjah ², Fadl A. Essa ⁴ 
and Ammar H. Elsheikh ^{5,*} 

¹ Mechanical Department, Faculty of Technology and Education, Beni-Suef University, Beni Suef 62511, Egypt

² Imam Mohammad Ibn Saud Islamic University, Riyadh 11432, Saudi Arabia

³ Powder Technology Department, Central Metallurgical Research and Development Institute CMRDI, Cairo 11865, Egypt

⁴ Mechanical Engineering Department, Faculty of Engineering, Kafrelsheikh University, Kafrelsheikh 33516, Egypt

⁵ Department of Production Engineering and Mechanical Design, Tanta University, Tanta 31527, Egypt

* Correspondence: ammar_elsheikh@f-eng.tanta.edu.eg

Abstract: The effect of tungsten, aluminum, and cobalt on the mechanical properties of iron-based composites prepared by powder technology was studied. Five samples with different contents of tungsten, aluminum, and cobalt were established. The five samples have the following chemical compositions: (I) full iron sample, (II) 5wt.% tungsten, (III) 5wt.% tungsten-4wt.% cobalt-1wt.% aluminum, (IV) 5wt.% tungsten-2.5wt.% cobalt-2.5wt.% aluminum, and (V) 5wt.% tungsten-1wt.% cobalt-4wt.% aluminum. The mixed composite powders were prepared by mechanical milling, in which 10:1 ball to powder ratio with 350 rpm for 20 h was cold compacted by a diaxial press under 80 bars, then sintered at temperatures ranging from 1050 °C to 1250 °C in an argon furnace. The samples were characterized mechanically and physically using XRD, SEM, a density measuring device, a hardness measuring device, a compression test device, and a tribological device for wear and friction tests. XRD results refer to the formation of different intermetallic compounds such as Fe₇W₆, Al₅Co₂, Fe₂W₂Co and Co₇W₆ with the main peaks of Fe. The good combination of tribological and mechanical properties was recorded for sample number five, which contained 5% W, 4% Al, 1% Co and Fe base, where it obtained the highest wear resistance, largest hardness, acceptable compressive strength, and lowest friction coefficient due to the good combination of hard and anti-friction intermetallic action compared with the other samples. This sample is a good candidate for applications which require high wear resistance and a moderate friction coefficient accompanied with high toughness, like bearing materials for both static and dynamic loading with superior mechanical and tribological properties.

Keywords: iron-based composites; tungsten; aluminum; cobalt; specific wear rate; coefficient of friction; microstructure; powder metallurgy



Citation: Mohammed, M.M.; Alrasheedi, N.H.; El-Kady, O.A.; Djuansjah, J.; Essa, F.A.; Elsheikh, A.H. Impact of Using Tungsten, Cobalt, and Aluminum Additives on the Tribological and Mechanical Properties of Iron Composites. *Crystals* **2023**, *13*, 395. <https://doi.org/10.3390/cryst13030395>

Academic Editor: Shouxun Ji

Received: 31 January 2023

Revised: 11 February 2023

Accepted: 22 February 2023

Published: 24 February 2023



Copyright: © 2023 by the authors. Licensee MDPI, Basel, Switzerland. This article is an open access article distributed under the terms and conditions of the Creative Commons Attribution (CC BY) license (<https://creativecommons.org/licenses/by/4.0/>).

1. Introduction

Developing composite materials with enhanced mechanical and tribological properties received considerable attention in recent years [1–3]. Both metal-based and polymer based composites have been extensively studied in literature [4–6] because of their enhanced properties over conventional alloys [7,8]. Bearing materials that can be used in high temperature applications have great attention from researchers [9,10], in which various types of iron-based composites were investigated. Iron powder has gained great attention from researchers in the last few decades [11–13] because it has many advantages over conventional ferrous alloys, such as superior mechanical properties arising from refined microstructure. Unfortunately, it has a low tribological properties, so reinforcing it with other additives such as ceramic metals or materials improves the wear resistance. Powder metallurgy is the most

suitable technique for the fabrication of these alloys, as it has the advantage of obtaining final shape or semi-final shape with low cost and better quality [14,15]. Some researchers work on these alloys such as Cui et al. [16], who added BaF₂, Ag and Mo to Fe-Cr matrix composites under different concentrations. They reported that the optimum tribological properties were obtained at 8% BaF₂, 10% Ag and 8.5% Mo. The effect of boron (B) on the mechanical properties of Fe-Cr matrix composites was investigated [17]. They found that the addition of B enhanced the tribological properties of this alloy. Suh et al. [18] added Multi Wall Carbon Nano Tube (MWCNT) to Fe-based composites. The results revealed that MWCNTs were decomposed at high temperature and reacted with iron to form an Fe-C interstitial phase alloy and lose their positive effect on the mechanical behavior of these alloys. Merie et al. [19] investigated the effect of TiO₂ addition on Fe-10% Cu-7% graphite-12% Ni composites for vehicle brake applications. The results stated that the porosity was increased with increasing TiO₂ content. Furthermore, the highest friction coefficient of 0.43 was recorded for 6% TiO₂, and the maximum wear resistance was obtained for 8% TiO₂. Tungsten (W) was added as a solid solution strengthening phase for α -Fe [20], in which W reacted with Fe and carbon to form iron tungstate (Fe₂W₂C, Fe₃W₃C and Fe₆W₆C). The formed phases acted as a bearing microstructure for the secondary lubricating films during the wear process. It was reported that Fe-W-C compounds were thermodynamically stable, and its elastic constants were larger than Fe₃C and Cr₇C₃. The high hardness of Fe-W-C ternary compounds is due to the mixed bonds, which are a combination of metallic and covalent bonds. Co has a similar influence to W on the properties of α -Fe, however Al acts as a binder and forms anti-friction layers. Kang et al. [21] fabricated Al matrix composites reinforced by Al-Fe-Cr using a laser powder bed fusion technique to produce a novel high strength composite. The fabricated samples had nano-quasicrystalline particles with various sizes for a heterogeneous microstructure. The produced composites have a high ultimate and yield strength of 530 MPa and 395 MPa, respectively. Gao et al. [22] fabricated Fe-Cr-B matrix composites reinforced by zirconia toughened alumina particles using a liquid-phase sintering technique. An interface film with 50 μ m thickness is generated between the Fe-Cr-B alloy and the used particles. The Young's modulus and hardness at the formed film are 146.60 GPa and 12.88, respectively, which augment the adhering between the composite components. The fabricated samples had outstanding wear resistance which increased as the particles' volume fraction increased. Pashangeh et al. [23] fabricated Al-matrix composites reinforced by Al-Cr-Fe using an accumulative roll bonding technique. The anti-corrosion characteristics of the fabricated samples was higher than monolithic Al. Somunkiran et al. [24] fabricated Fe-Cr matrix composites reinforced by C or C-B using a hot pressing technique. The density and hardness of the fabricated samples changed by the reinforcement elements. C-B reinforced samples had higher density and hardness than those reinforced by C. Kang et al. [25], who fabricated Al matrix composite samples reinforced by Al-Fe-Cr using a selective laser melting technique. The size of reinforcement elements increased from nanometer scale to micrometer scale, and its structure converted from dense structure to porous structure with increasing laser power. Chen et al. [26] studied the tribological behavior of Fe-Ni composites considering Ni-coated reduced graphene oxide-MoS₂ fabricated by powder metallurgy. The results concluded that Ni-coated reduced graphene oxide-MoS₂ composites retained their outstanding tribological properties at higher temperatures. Bai et al. [27] studied the influence of adding V₈C₇ to iron composites by in-situ reaction in two steps. They found that V₈C₇-iron composites achieved higher yield strength and compressive strength compared to using cast iron with the same chemical composition and V₈C₇ area fraction. Jiang et al. [28] examined two types of high Cr white iron composites with TiC added either in dried or in-situ. They found that the TiC_x in situ prepared composites exhibited superior mechanical and tribological properties compared with the directly added TiC. This is due to the smaller grain size and stronger interfacial strength obtained in the in-situ samples. Most of the alloys mentioned above are expensive and the manufacturing techniques are costly as well.

The main aim of this work is to develop a new generation of composite material with high mechanical and tribological properties that could be used as bearing material applications with reasonable cost by investigating the effect of adding W, Co, and Al on the mechanical and tribological behaviors of an Fe-based matrix. Fe powder with fixed W content (5%) and various Al and Co contents will be prepared. Adjusting the stoichiometric amounts of Al and Co is the biggest challenge to achieving the optimal mechanical properties. The tribological, physical, and mechanical characteristics were tested to figure out the role of different reinforcement materials on the composite structure and to determine the optimal composition.

2. Experimentation

The procedures of the experimental study are presented in Figure 1, which includes the material selection to obtain samples with diverse weight percentages of Al, Co, and W in which the W content was kept constant. The main reason behind the addition of W element to Fe powder was to increase the strength and thermal stability of the produced material, as W is a ceramic metal has high mechanical properties and good thermal stability [29]. The addition of Co element improves the ductility of the final product and forms a new intermetallic material with Fe or W [30]. Finally, the addition of Al enhances the ductility and thermal properties [31]. Mechanical milling of the powders by 1:10 powder-to-ball ratio and 350 rpm for 20 h was used to reach the desired grain size and to get homogeneous distribution of the ingredients. The mixed powders were cold compacted using hydraulic press under 80 bars with a bi-axial die (10.5 ± 0.1 mm diameter and 0.5 ± 0.1 mm height). The compacted samples, after cold pressing, were sintered at different temperatures of 1050, 1100, 1200, and 1250 °C for 60 min to complete the sintering process under an Argon atmosphere in order to protect samples from any oxidation. This wide range of sintering temperatures enables us to figure out the effects of sintering temperatures on the different properties of the fabricated samples. According to the rule of mixtures, sintering temperature ranges between 1050 up to 1250 °C, so we used this temperature range to check which one is more suitable and gives the highest densification. The effect of sintering temperature on the density values was studied, as this is the most important parameter for the powder metallurgy products. The samples were investigated according to standard, in which five different specimens were produced by employing the technique of powder metallurgy with the chemical contents in Table 1. These compositions are selected as there is no previous work done on these compositions; furthermore, constant percentage of W (5%) is enough for improving the properties of iron. For Al-Co percentages, these ratios are suitable for investigating the influence of Al and Co on the composite properties.

Table 1. Chemical composition of the prepared samples.

Material	wt. %				
	Specimen #1	Specimen #2	Specimen #3	Specimen #4	Specimen #5
Fe	100%	95%	90%	90%	90%
W	-	5%	5%	5%	5%
Co	-	-	4%	2.5%	1%
Al	-	-	1%	2.5%	4%

Sample 1 was prepared to be a reference sample, while 5wt.% W was kept constant for all other samples, as this content is completely dissolved in Fe as a solid solution in the temperature range from 1000 to 1250 °C according to the Fe-W phase diagram. Co and Al were varied in samples 3 to 5 to obtain the optimum weight percentage needed for Co-Al intermetallic formation according to their binary phase diagram.

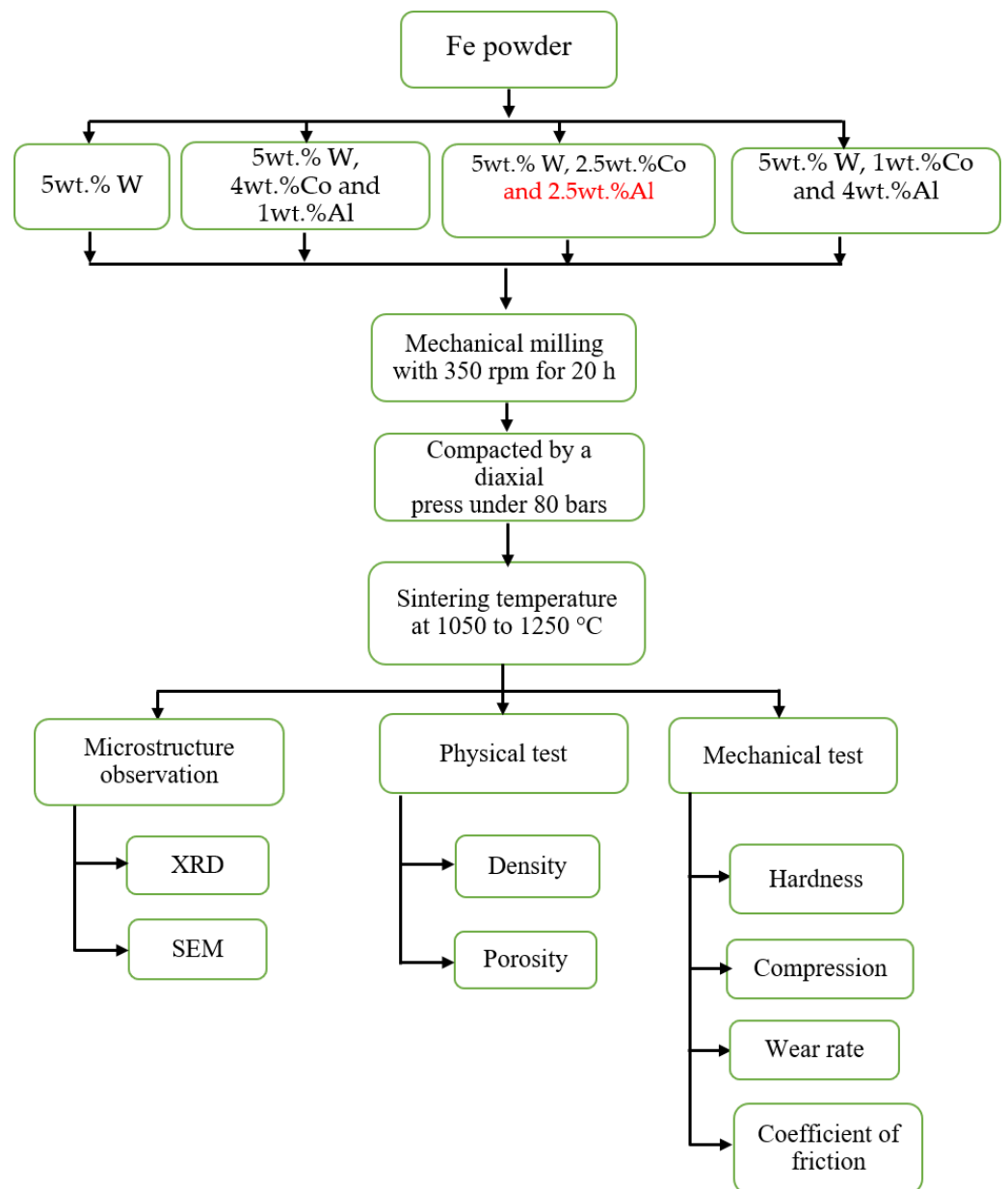


Figure 1. Flow chart of the experimental procedures.

3. Characterizations

3.1. Density of Sintered Samples

Density is an important parameter for powder metallurgy samples. Actual density was determined by Archimedes' method by using water as a floating liquid as following:

$$\text{Actual density} = \frac{W_{\text{air}}}{W_{\text{air}} - W_{\text{H}_2\text{O}}} \left(\text{gm/cm}^3 \right) \quad (1)$$

where, W_{air} and $W_{\text{H}_2\text{O}}$ are the weights in air and water, respectively. Molten wax of known density was used to cover the sample's surface with a thin film to isolate the surface porosity that exists on it, and then weighted again in air.

Theoretical density was calculated according to density:

$$(\rho) = \frac{\text{mass, (m)}}{\text{volume, (v)}} \left(\text{gm/cm}^3 \right) \quad (2)$$

Finally, the relative density is calculated as the actual density of sample/the theoretical density.

3.2. Microstructure Investigation

A scanning electron microscope with an EDX unit (JEOL, JSE-T20) was used to investigate the grains which formed after the sintering process, and to identify the intermetallic compounds formed during sintering, taking into consideration the precautions in [32–34]. Furthermore, the particle shape and size, grain boundaries, and porosity were investigated.

3.3. Mechanical Properties

3.3.1. Compressive Testing

Compressive testing was conducted on a universal testing machine, model UH-500 KNA, Schematzu, using test specimens 10.4 mm in diameter.

3.3.2. Surface Hardness

Surface micro hardness was measured using Vickers hardness tester MH-5 with 300 g load and 10 s dwell time. An average of 5 measurements for each specimen was computed and considered as the final measured value.

3.4. Tribological Testing

Tribological tests were executed on a Pin-On-Disk machine to obtain the specific wear rate and friction coefficient. The disk was made of alloyed grey cast iron.

3.4.1. Friction Coefficient

The friction coefficient was computed considering a sliding speed of 7 m/s and friction force of 42 N.

3.4.2. Wear Rate

Specific wear rate defines the reduction of the specimen mass as a measure of wear with respect to time, and it is computed using the following formula:

$$\text{Specific Wear Rate (SWR)} = \frac{\Delta W}{\rho \times V \times T \times F_f} \quad (\text{cm}^3/\text{N.m}) \quad (3)$$

where T: test duration (s), Δw : weight difference (gm), ρ : density, (gm/cm³), F_f : friction force (N), and V: sliding speed (m/s).

A constant applied load of 42 N was considered. The conditions of tribological tests are given in Table 2.

Table 2. Tribological testing conditions.

Sample area	85 mm ²	Test duration	18 min
Sliding speed	7 m/s	Ambient temperature	25 °C
Friction pressure	0.5 MPa		

The lower wear rates are a direct indicator to the high resistance of the material to abrasion and wear, which is desirable characteristic for bearing materials. The chemical composition of the disk used in tribological testing is tabulated in Table 3.

Table 3. Composition of the disk.

C %	Mn %	Si %	S %	Ni %	Cr %	Mo %
3.3–3.5	0.6–0.9	1.8–2.1	0.12	0.6–0.7	0.15–0.25	0.2–0.3

4. Results and Discussion

4.1. Composition and Phase Structure

Figure 2 shows the XRD of S₂, S₃, S₄ and S₅ samples. It shows that sample two contains peaks corresponding to an Fe and Fe₂W₆ intermetallic that formed during the sintering process. For all samples that contain Fe, W, Co, and Al, the main peaks of Fe metal strongly appeared. Co₃W₆, Fe₂W₃, Co, and Al₅Co₂ peaks are also observed. According to the Co-W and Co-Al binary diagrams, and the ternary diagram of Fe, W, and Co, some intermetallic compounds are formed during the sintering process at certain temperatures and concentrations. For Co₃W₆, Fe₂W₃Co and Al₅Co₂ intermetallic compounds, their peak intensities are increased by increasing the percent of both Co and Al [35]. Alumina phases are also formed during the exposure of the samples to oxygen-containing environments at high temperature. Furthermore, as-received Al powder contained some Al₂O₃ particles.

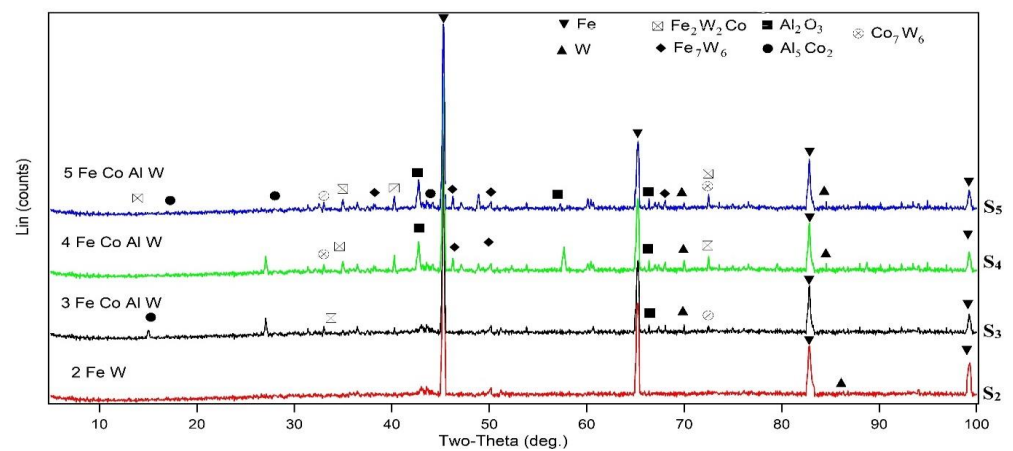


Figure 2. XRD pattern of S₂, S₃, S₄ and S₅.

4.2. Density Estimation

All samples are sintered at 1050, 1100, 1200, and 1250 °C in an Ar atmosphere furnace. By measuring their densities, the results showed that 1050, 1100 and 1200 °C are not suitable temperatures to complete the sintering process, and the density was very low, ranging between 70–80%. For 1250 °C, the density was raised more than 90%. Therefore, 1250 °C is the most suitable temperature. Figure 3 shows the effect of metal additions with different percentages on the relative density of the Fe matrix. It is clear that the addition of 5wt.% tungsten (W) decreased the density of Fe, although W had a higher density value than Fe (19.4 gm/cm³ compared to 7.8 gm/cm³). This may be because of the existence of pores, formed from W particle agglomerations due to the large difference in the melting points between Fe and W: 1538 and 3422 °C, respectively, which is clear in the resulting microstructure. By adding Co and Al (4% and 1%, respectively) to the Fe-W alloy, the density was increased again in sample three due to the liquid phase sintering established by the melting of Al at 663 °C during the sintering process. The presence of the liquid phase increased the densification, as liquid Al spreads in the alloy matrix and fills the internal voids between the particles. Consequently, densification improved. The addition of equal amounts of Al and Co (2.5% for each) enhanced the densification again. This may be due to the increase in Al liquid phase and the formation of Fe₂W₂Co intermetallic phase, which both have a high density. However, by decreasing the Co to 1% in sample 5, the density was decreased, which may be due to three factors; the first is the increase in Al content which has lower density (2.7 gm/cc) than the other contents, and the second is the agglomerations which were observed in the microstructure. The third factor is the reduction in the Co content, which results in decreasing the area fraction of Fe₂W₂Co intermetallic compounds. In statistics, standard deviation is a measure of the quantity of dispersion or deviation of a set of values. Figure 4 illustrates the effect of standard deviation on all samples.

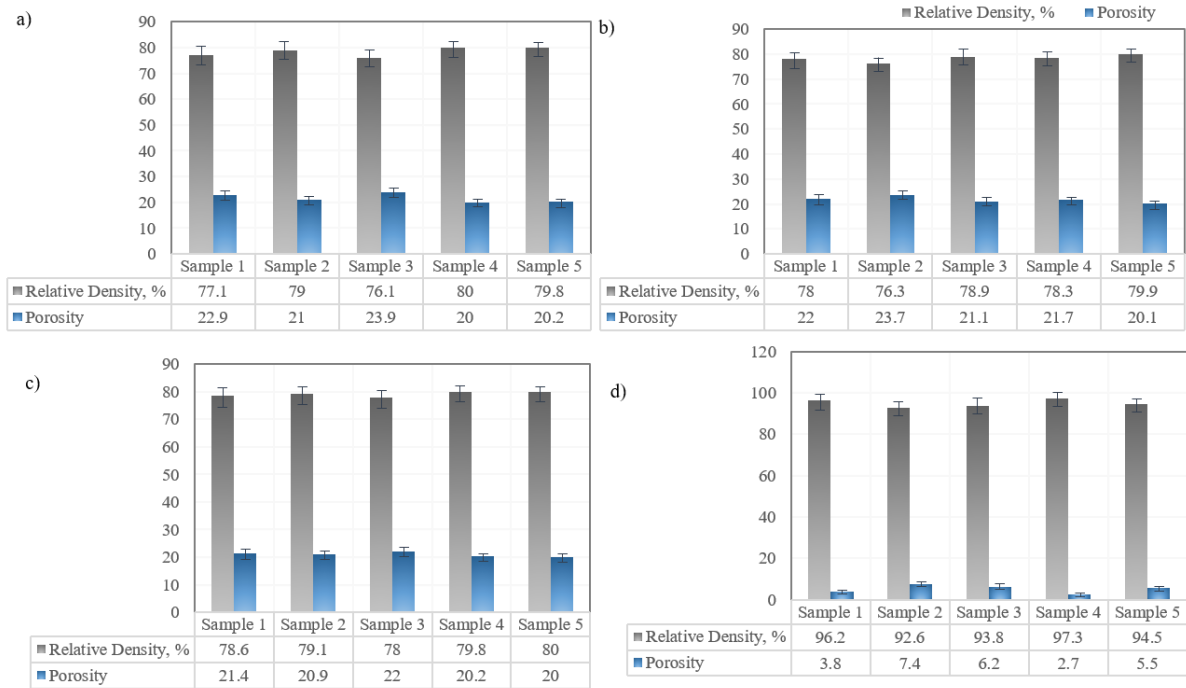


Figure 3. Variation of relative density of the different samples; (a) Specimen #2; (b) Specimen #3; (c) Specimen #4; (d) Specimen #5.

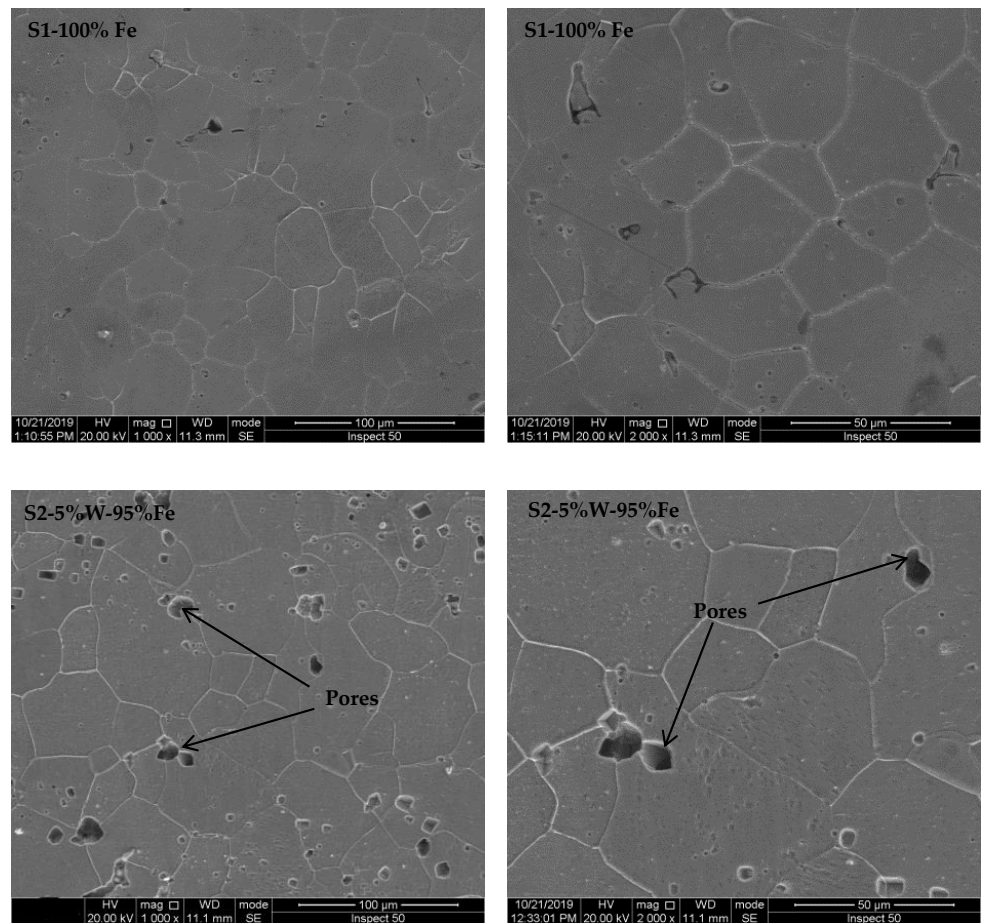


Figure 4. Microstructures of samples 1 and 2 at two different magnifications.

4.3. Microstructure Investigation

Figure 5 shows the microstructure of all samples after sintering at 1250 °C at two different magnifications of 1000X and 2000X for each sample. The most predominant phase is the grey one, which represents the Fe matrix. Well-defined grain boundaries were obtained and some pores at the surface for sample 1 (100% Fe) were observed. Sample 2 obtained similar trends to sample 1, which was an indication of 100% full densification but with a higher area fraction of pores.

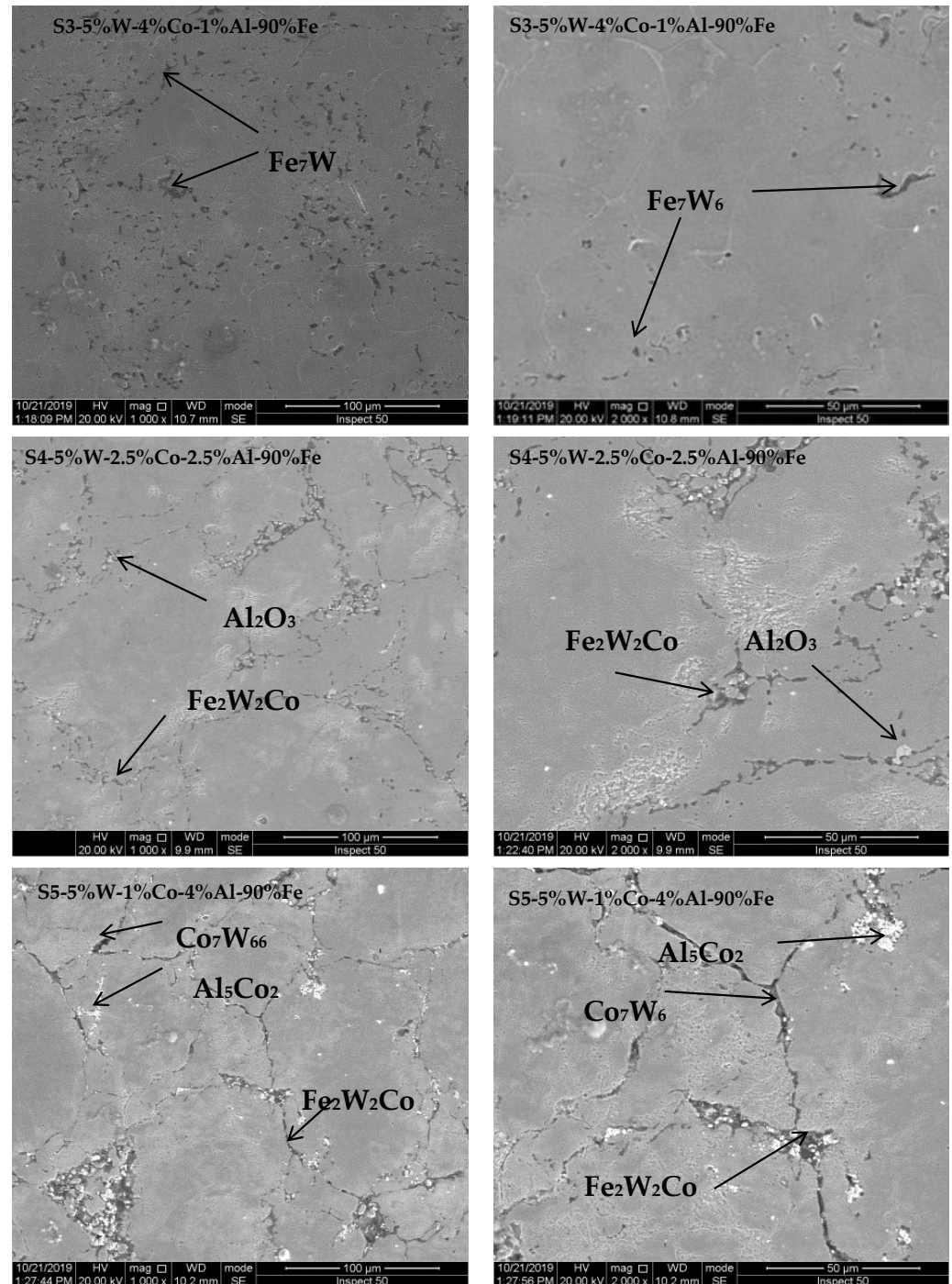


Figure 5. Microstructures of samples 3, 4, and 5 at two different magnifications.

The area fraction of pores in 5%W added sample was higher than that of the pure iron sintered sample, which implies that W in solid solution increased the porosity. This may be due to the agglomeration resulting from the large difference in melting points between iron and tungsten that was confirmed also from the density results [20]. Sample 3 (90%Fe-5%W-4%Co-1%Al) contains well-defined grain boundaries decorated with intermetallic material between Fe, Co and W, which imply that 4%Co and 1%Al enhance the precipitation of intermetallic material at the grain boundaries. Sample 4 (90%Fe-5%W-2.5%Co-2.5%Al) shows almost no pores. Intermetallics of Fe, W, Co, and Al are formed along the grain boundaries and inside the grains; the stoichiometric amounts of (90%Fe-5%W-2.5%Co-2.5%Al) increases the intermetallic area fraction in this sample. Sample 5 (90%Fe-5%W-1%Co-4%Al) shows the largest area fraction of intermetallic material (Al_5Co_2 ; Co_7W_6 and $\text{Fe}_2\text{W}_2\text{Co}$), which was confirmed by XRD and EDX analysis of material that was found along the grain boundaries and inside the grains. This confirmed that the stoichiometric amounts of (90%Fe-5%W-1%Co-4%Al) gives the optimum composition to achieve the largest area fraction of intermetallic material in this sample. Co_7W_6 and $\text{Fe}_2\text{W}_2\text{Co}$ act as a bearing microstructure for the secondary lubricating films during the wear process [20], while Al_5Co_2 acts as an anti-friction particle. From the microstructure images, it is clear that the most densified sample that has the lowest porosity and more fine particles is S4, which contains an equal percentage of Co and Al (2.5 and 2.5 ratio).

5. Effect of W, Al and Co on the Properties of Bearing Material

Vickers Hardness

The obtained results of surface hardness are presented in Figure 6. The hardness was augmented by the addition of W, Co and Al gradually. Sample 5 (90%Fe-5%W-4%Al-1%Co) recorded the largest hardness (194 HV), which may be due to the large area fraction of intermetallics formed in this sample. The high hardness is highly desirable for materials with high resistance to abrasion and wear. The addition of W to Fe improves the total hardness of the prepared composites [36]. This is due to the higher hardness value of W compared to Fe, and the good distribution of W all over the Fe matrix. Furthermore, W is a ceramic metal that acts as an internal ball which causes a grain reinforcement of the particles. Consequently, the hardness was improved according to the Hall–Petch equation. Al acts as an internal binder which melts at 663 °C during the sintering process and fills the internal pores, so the hardness was increased. Moreover, the formed Fe_7W_6 , $\text{Fe}_2\text{W}_2\text{Co}$, Co_7W_6 , and Al_5Co_2 intermetallics have a good role in enhancing the hardness.

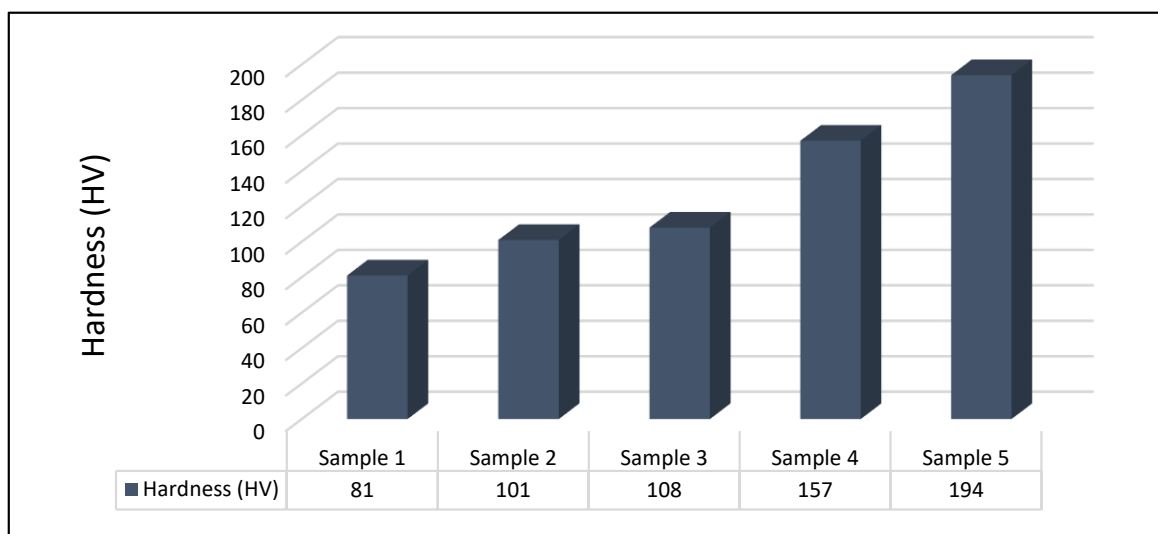


Figure 6. The variation of hardness for different samples.

6. Compressive Strength

The compressive strength is shown in Figure 7. Compressive strength has been increased from 270 MPa to 360 MPa by the addition of (5% W (as a result of Fe_7W_6 solid solution strengthening, and the high hardness of W metal. Further addition of Al and Co does not greatly affect the compressive strength for samples three and four. Both of them increased the compressive strength, but by a low percentage. This may be due to the liquefaction of Al at $663\text{ }^\circ\text{C}$ which fills the internal pores. Consequently, the compressive strength enhanced as the weakness effect of the voids is excluded. However, Co is a ductile metal, and its presence reduced the strength of the samples. Sample five shows a slight decrease in compressive strength by 3% due to the relatively large content of Al (4%), which acts as a filler material and intermetallic forming element. This slight decrease in compressive strength accompanied with the largest hardness, largest wear resistance and minimum friction coefficient make sample five a promising material for both static and dynamic bearings.

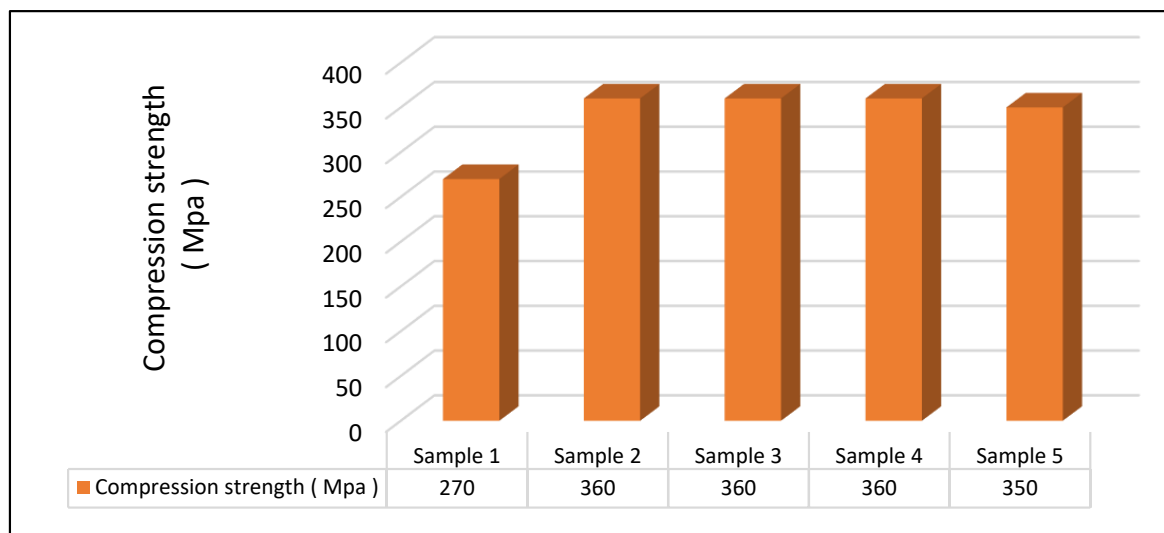


Figure 7. Compressive strength for all sintered samples.

6.1. Specific Wear Rate

Figure 8 shows the effect of W, Co, and Al additions on the wear rate of iron matrix. From Figure 6, one can notice a gradual decrease of the wear rate by increasing the additive metals. The addition of W increased the wear resistance, as W is a hard-ceramic metal that strengthens the Fe matrix and increases the hardness of iron due to its good homogeneous distribution through the Fe matrix [22]. The addition of both Co and Al increased the wear resistance due to the formation of intermetallic phases and the liquefaction of Al during the sintering process, which increases the densification and consequently improves the wear resistance. Sample five (90% Fe-5%W-4%Al-1%Co) obtained the largest wear resistance and the largest hardness (194 HV) due to the high content of Al discussed above.

6.2. Friction Coefficient

The friction coefficient variation as a function of time is shown in Figure 9. The lowest friction coefficient after reaching a steady state was recorded for sample five, which shows the largest hardness and the largest wear resistance, implying a promising candidate for bearing materials applications. This can be explained by the high wear resistance of this sample. The friction coefficient was usually decreased by increasing the wear resistance, as the hard surface of the sample resists scratches. This may be due to the formation of Al_5Co_2 , which acts as an anti-friction particle. Furthermore, reinforcing the Fe matrix with W improves the overall strength of the prepared samples due to its ceramic nature and high hardness. The material tested in Sample five (5% W, 1% Co, 4% Al) can be used for bearing

materials application, as it serves at severe tribological and mechanical conditions for both static and dynamic loadings, in which all the intermetallics formed are thermodynamically stable up to 400 °C. Additionally, the formed intermetallic phases increased the strength of the samples and its resistance to scratches. A good interaction between the constituents is established.

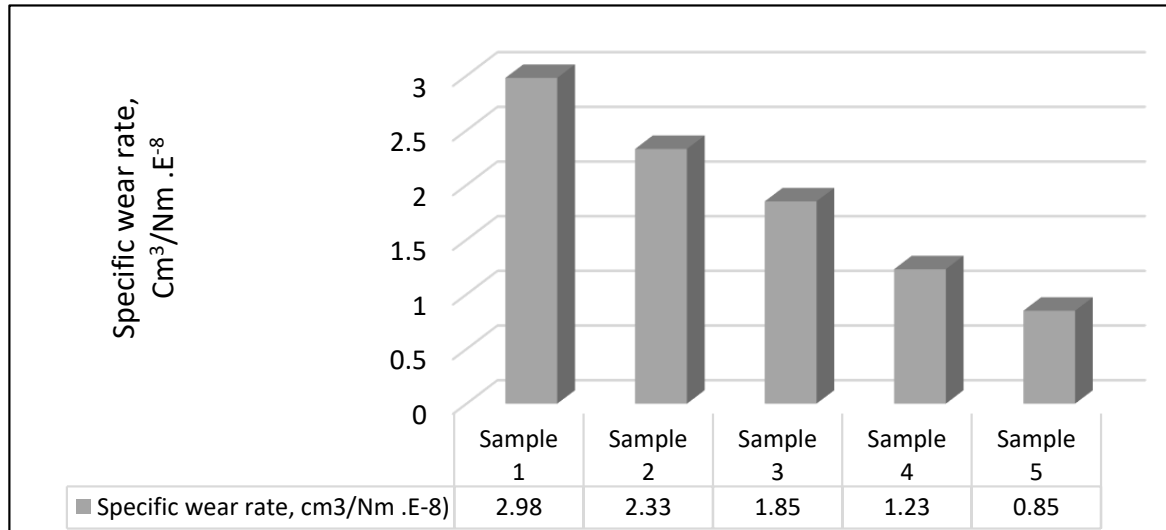


Figure 8. Wear rates for all sintered samples.

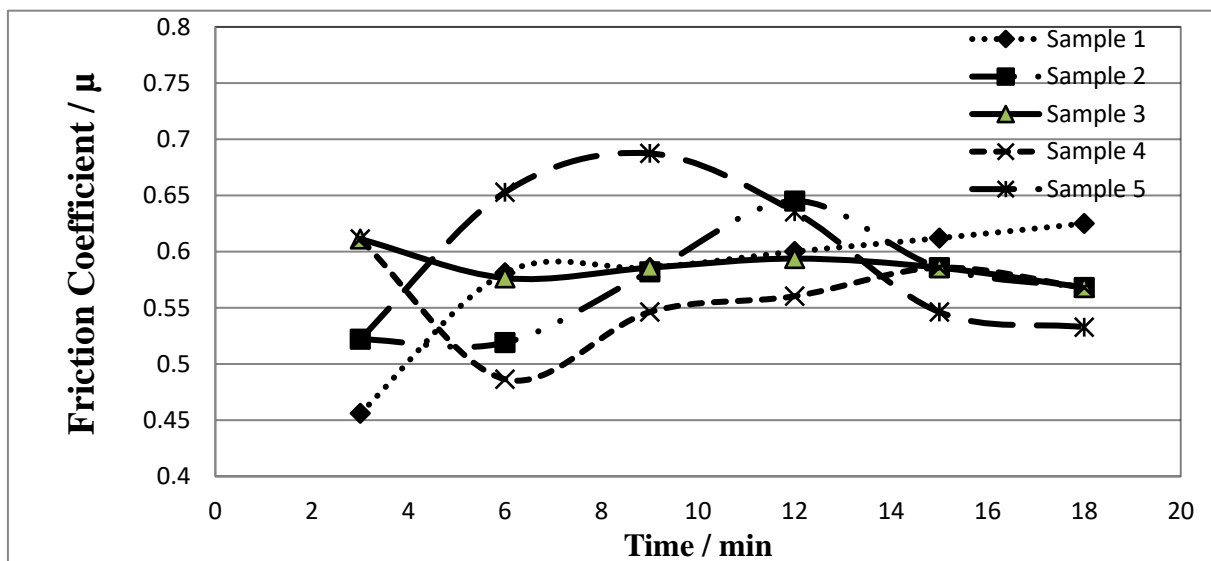


Figure 9. Variation of friction coefficient with test duration.

6.3. Comparison Overview

The test results of all specimens are in Table 4. The results were computed as the average of five testing reads for each condition. By comparing the friction coefficient of pure Fe and the other samples containing W, Co, and Al, it is clear that the friction coefficient was decreased by these additions due to the presence of W powder with its ceramic nature, helping reduce the friction coefficient. The use of aluminum with a high weight fraction (4wt.%) boosted the hardness, minimized the friction coefficient as well as wear rate, and increased the material strength to reasonable value. In our future work, we will employ different machine learning models such as multilayer perceptron, random vector functional

link, support vector machine, random forest, and recurrent neural networks [37–39] to predict the properties of the fabricated samples under different material contents.

Table 4. Characteristics of the tested bearing materials.

Materials	Specimen #1	Specimen #2	Specimen #3	Specimen #4	Specimen #5
W content, wt.%	0%	5%	5%	5%	5%
Co content, wt.%	0%	0%	4%	2.5%	1%
Al content, wt.%	0%	0%	1%	2.5%	4%
Relative Density, %	96.2	92.6	93.8	97.3	94.5
Standard Deviation	7.94	6.36	7.06	7.79	6.32
Compressive strength, MPa	270	360	360	360	350
Hardness, HV	81	101	108	157	194
Friction coefficient	0.62	0.58	0.57	0.57	0.53
Specific wear rate, SWR, cm ³ /Nm	2.98×10^{-8}	2.33×10^{-8}	1.85×10^{-8}	1.23×10^{-8}	0.85×10^{-8}

7. Conclusions

Fe powder mixed with constant W content (5%) and different Co and Al contents has been produced by powder metallurgy. Sintering temperature was varied between 1050 to 1250 °C. Higher temperatures resulted in liquid phase formation, while lower temperatures resulted in incomplete sintering, and the optimum suitable sintering temperature was 1250 °C, which was selected as sintering temperature for all prepared samples. Generally, the addition of W, Co, and Al to an Fe matrix enhanced the mechanical properties of the produced composites. The following conclusions could be deduced:

- (1) The relative density was slightly affected by the W, Co, and Al additions. All produced composites had relative density ranges from (93~97.4%).
- (2) The highest relative density (97.4%) was obtained for the composite that contained 5% W, 2.5% Co, and 2.5% Al.
- (3) XRD results indicated the formation of intermetallic compounds between Fe, W, Co, and Al which improved the mechanical properties.
- (4) The largest hardness (192 HV) was obtained for the composite that contained 5% W, 1% Co, and 4% Al, which is higher than that of a pure Fe matrix by about 240%.
- (5) Compressive strength was affected greatly by the addition of 5% W, which was increased by 35% compared to pure Fe powder, and this increase was slightly affected by Al and Co additions.
- (6) The composite that contained 5% W, 1% Co, and 4% Al had the largest hardness, the largest wear resistance, and the lowest friction coefficient when compared with a pure Fe matrix. This composite (5% W, 1% Co, 4% Al) is a good candidate for bearing materials at severe mechanical and tribological conditions for both static and dynamic loadings.

Author Contributions: All authors contributed equally. All authors have read and agreed to the published version of the manuscript.

Funding: The authors extend their appreciation to Imam Mohammad Ibn Saud Islamic University for funding this research with grant no. RG-21-12-01.

Acknowledgments: The authors extend their appreciation to Imam Mohammad Ibn Saud Islamic University for funding this research with grant no. RG-21-12-01.

Conflicts of Interest: The authors declare no conflict of interest.

References

1. Elsheikh, A.H.; Abd Elaziz, M.; Ramesh, B.; Egiza, M.; Al-qaness, M.A.A. Modeling of Drilling Process of GFRP Composite Using a Hybrid Random Vector Functional Link Network/Parasitism-Predation Algorithm. *J. Mater. Res. Technol.* **2021**, *14*, 298–311. [[CrossRef](#)]
2. Showaib, E.A.; Elsheikh, A.H. Effect of Surface Preparation on the Strength of Vibration Welded Butt Joint Made from PBT Composite. *Polym. Test.* **2020**, *83*, 106319. [[CrossRef](#)]
3. Thangaraj, M.; Ahmadein, M.; Alsaleh, N.A.; Elsheikh, A.H. Optimization of Abrasive Water Jet Machining of SiC Reinforced Aluminum Alloy Based Metal Matrix Composites Using Taguchi–DEAR Technique. *Materials* **2021**, *14*, 6250. [[CrossRef](#)] [[PubMed](#)]
4. Elsheikh, A.H.; Panchal, H.; Shanmugan, S.; Muthuramalingam, T.; El-Kassas, A.M.; Ramesh, B. Recent Progresses in Wood-Plastic Composites: Pre-Processing Treatments, Manufacturing Techniques, Recyclability and Eco-Friendly Assessment. *Clean. Eng. Technol.* **2022**, *8*, 100450. [[CrossRef](#)]
5. Kamal, A.; Ashmawy, M.; Algazzar, A.M.; Elsheikh, A.H. Fabrication Techniques of Polymeric Nanocomposites: A Comprehensive Review. *Proc. Inst. Mech. Eng. Part C J. Mech. Eng. Sci.* **2021**, *236*, 4843–4861. [[CrossRef](#)]
6. Abu-Okail, M.; Alsaleh, N.A.; Farouk, W.M.; Elsheikh, A.; Abu-Oqail, A.; Abdelraouf, Y.A.; Ghafaar, M.A. Effect of Dispersion of Alumina Nanoparticles and Graphene Nanoplatelets on Microstructural and Mechanical Characteristics of Hybrid Carbon/Glass Fibers Reinforced Polymer Composite. *J. Mater. Res. Technol.* **2021**, *14*, 2624–2637. [[CrossRef](#)]
7. Elsheikh, A.H.; Guo, J.; Huang, Y.; Ji, J.; Lee, K.-M. Temperature Field Sensing of a Thin-Wall Component during Machining: Numerical and Experimental Investigations. *Int. J. Heat Mass Transf.* **2018**, *126*, 935–945. [[CrossRef](#)]
8. Elsheikh, A. Bistable Morphing Composites for Energy-Harvesting Applications. *Polymers* **2022**, *14*, 1893. [[CrossRef](#)]
9. Liu, Y.; Jiang, Y.; Zhou, R.; Feng, J. First-Principles Calculations of the Mechanical and Electronic Properties of Fe–W–C Ternary Compounds. *Comput. Mater. Sci.* **2014**, *82*, 26–32. [[CrossRef](#)]
10. Zhou, H.; Wu, C.; Tang, D.; Shi, X.; Xue, Y.; Huang, Q.; Zhang, J.; Elsheikh, A.H.; Ibrahim, A.M.M. Tribological Performance of Gradient Ag-Multilayer Graphene/TC4 Alloy Self-Lubricating Composites Prepared by Laser Additive Manufacturing. *Tribol. Trans.* **2021**, *64*, 819–829. [[CrossRef](#)]
11. Li, Y.; Gao, Y. Three-Body Abrasive Wear Behavior of CC/High-Cr WCI Composite and Its Interfacial Characteristics. *Wear* **2010**, *268*, 511–518. [[CrossRef](#)]
12. Essa, F.A.; Yu, J.; Elsheikh, A.H.; Tawfik, M.M. A New M50 Matrix Composite Sintered with a Hybrid SnS/ZnO Nanoscale Solid Lubricants: An Experimental Investigation. *Mater. Res. Express* **2019**, *6*, 116523. [[CrossRef](#)]
13. Elsheikh, A.H.; Yu, J.; Sathyamurthy, R.; Tawfik, M.M.; Shanmugan, S.; Essa, F.A. Improving the Tribological Properties of AISI M50 Steel Using SnS/ZnO Solid Lubricants. *J. Alloys Compd.* **2020**, *821*, 153494. [[CrossRef](#)]
14. Ahmadein, M.; El-Kady, O.A.; Mohammed, M.M.; Essa, F.A.; Alsaleh, N.A.; Djuansjah, J.; Elsheikh, A.H. Improving the Mechanical Properties and Coefficient of Thermal Expansion of Molybdenum-Reinforced Copper Using Powder Metallurgy. *Mater. Res. Express* **2021**, *8*, 96502. [[CrossRef](#)]
15. Mohammed, M.M.; Elsayed, E.M.; El-Kady, O.A.; Alsaleh, N.A.; Elsheikh, A.H.; Essa, F.A.; Ahmadein, M.; Djuansjah, J. Electrochemical Behavior of Cu-MWCNT Nanocomposites Manufactured by Powder Technology. *Coatings* **2022**, *12*, 409. [[CrossRef](#)]
16. Cui, G.; Lu, L.; Wu, J.; Liu, Y.; Gao, G. Microstructure and Tribological Properties of Fe–Cr Matrix Self-Lubricating Composites against Si₃N₄ at High Temperature. *J. Alloys Compd.* **2014**, *611*, 235–242. [[CrossRef](#)]
17. Cui, G.; Kou, Z. The Effect of Boron on Mechanical Behavior and Microstructure for Fe–Cr Matrix Alloy Prepared by P/M. *J. Alloys Compd.* **2014**, *586*, 699–702. [[CrossRef](#)]
18. Suh, J.Y.; Bae, D.H. Mechanical Properties of Fe-Based Composites Reinforced with Multi-Walled Carbon Nanotubes. *Mater. Sci. Eng. A* **2013**, *582*, 321–325. [[CrossRef](#)]
19. Merie, V.V.; Căndea, V.C.; Bîrleanu, C.; Pășcuță, P.; Popa, C.O. The Influence of Titanium Dioxide on the Tribological Characteristics of a Fe-Based Friction Composite Material. *J. Compos. Mater.* **2014**, *48*, 235–243. [[CrossRef](#)]
20. Kostornov, A.G.; Fushchich, O.I.; Chevychelova, T.M.; Kostenko, A.D.; Karpets, M. V Tribological Characteristics of the Iron-Based Composite at 500 C. *Powder Metall. Met. Ceram.* **2014**, *53*, 411–416. [[CrossRef](#)]
21. Kang, N.; Zhang, Y.; El Mansori, M.; Lin, X. Laser Powder Bed Fusion of a Novel High Strength Quasicrystalline Al–Fe–Cr Reinforced Al Matrix Composite. *Adv. Powder Mater.* **2023**, *2*, 100108. [[CrossRef](#)]
22. Gao, J.; Li, T.; Yan, Z.; Liu, S.; Zhao, Y.; Tong, W. Research on the Interface and Properties of Spherical ZTA Particles Reinforced Fe–Cr–B Matrix Composite. *J. Mater. Res. Technol.* **2022**, *19*, 1322–1331. [[CrossRef](#)]
23. Pashangeh, S.; Alizadeh, M.; Amini, R. Structural and Corrosion Behavior Investigation of Novel Nano-Quasicrystalline Al–Cr–Fe Reinforced Al-Matrix Composites Produced by ARB Process. *J. Alloys Compd.* **2022**, *890*, 161774. [[CrossRef](#)]
24. Somunkiran, I.; Buytoz, S.; Dagdelen, F. Determination of Curie Temperatures and Thermal Oxidation Behavior of Fe–Cr Matrix Composites Produced by Hot Pressing. *J. Alloys Compd.* **2019**, *777*, 302–308. [[CrossRef](#)]
25. Kang, N.; Fu, Y.; Coddet, P.; Guelorget, B.; Liao, H.; Coddet, C. On the Microstructure, Hardness and Wear Behavior of Al–Fe–Cr Quasicrystal Reinforced Al Matrix Composite Prepared by Selective Laser Melting. *Mater. Des.* **2017**, *132*, 105–111. [[CrossRef](#)]
26. Chen, B.; Li, X.; Jia, Y.; Li, X.; Zhang, M.; Dong, J. Tribological Properties of Fe–Ni-Based Composites with Ni-Coated Reduced Graphene Oxide–MoS₂. *J. Compos. Mater.* **2018**, *52*, 2631–2639. [[CrossRef](#)]

27. Bai, H.; Zhong, L.; Cui, P.; Lv, Z.; Xu, Y. Preparation of V8C7-Fe/Iron Dual-Scale Composite via Two-Step in Situ Reaction. *J. Mater. Res. Technol.* **2020**, *9*, 4114–4122. [[CrossRef](#)]
28. Jiang, J.; Li, S.; Hu, S.; Zhang, J.; Yu, W.; Zhou, Y. Comparison of High Cr White Iron Composites Reinforced with Directly Added TiC and in Situ Formed TiCx. *J. Mater. Res. Technol.* **2020**, *9*, 3140–3148. [[CrossRef](#)]
29. Wei, A.; Tang, Y.; Tong, T.; Wan, F.; Yang, S.; Wang, K. Effect of WC on Microstructure and Wear Resistance of Fe-Based Coating Fabricated by Laser Cladding. *Coatings* **2022**, *12*, 1209. [[CrossRef](#)]
30. Li, X.; Shi, Y.; Wang, S. Investigation of the Phase Transformation Characteristics of Fe-Co Elastocaloric Refrigeration Alloy. *J. Phys. Conf. Ser.* **2021**, *2076*, 12033. [[CrossRef](#)]
31. Zhang, Z.; Fan, G.; Tan, Z.; Zhao, H.; Xu, Y.; Xiong, D.; Li, Z. Towards the Strength-Ductility Synergy of Al₂O₃/Al Composite through the Design of Roughened Interface. *Compos. Part B Eng.* **2021**, *224*, 109251. [[CrossRef](#)]
32. De Groot, P.J. The Meaning and Measure of Vertical Resolution in Optical Surface Topography Measurement. *Appl. Sci.* **2017**, *7*, 54. [[CrossRef](#)]
33. Podulka, P. Selection of Methods of Surface Texture Characterisation for Reduction of the Frequency-Based Errors in the Measurement and Data Analysis Processes. *Sensors* **2022**, *22*, 791. [[CrossRef](#)] [[PubMed](#)]
34. Haitjema, H. Uncertainty in Measurement of Surface Topography. *Surf. Topogr. Metrol. Prop.* **2015**, *3*, 35004. [[CrossRef](#)]
35. Zhang, X.; Lai, L.; Xiao, S.; Zhang, H.; Zhang, F.; Li, N.; Guo, S. Effect of W on the Thermal Stability, Mechanical Properties and Corrosion Resistance of Fe-Based Bulk Metallic Glass. *Intermetallics* **2022**, *143*, 107485. [[CrossRef](#)]
36. Elsayed, A.; Li, W.; El Kady, O.A.; Daoush, W.M.; Olevsky, E.A.; German, R.M. Experimental Investigations on the Synthesis of W-Cu Nanocomposite through Spark Plasma Sintering. *J. Alloys Compd.* **2015**, *639*, 373–380. [[CrossRef](#)]
37. Elsheikh, A.H.; El-Said, E.M.S.; Abd Elaziz, M.; Fujii, M.; El-Tahan, H.R. Water Distillation Tower: Experimental Investigation, Economic Assessment, and Performance Prediction Using Optimized Machine-Learning Model. *J. Clean. Prod.* **2023**, *388*, 135896. [[CrossRef](#)]
38. Moustafa, E.B.; Elsheikh, A. Predicting Characteristics of Dissimilar Laser Welded Polymeric Joints Using a Multi-Layer Perceptrons Model Coupled with Archimedes Optimizer. *Polymers* **2023**, *15*, 233. [[CrossRef](#)]
39. Khoshaim, A.B.; Moustafa, E.B.; Bafakeeh, O.T.; Elsheikh, A.H. An Optimized Multilayer Perceptrons Model Using Grey Wolf Optimizer to Predict Mechanical and Microstructural Properties of Friction Stir Processed Aluminum Alloy Reinforced by Nanoparticles. *Coatings* **2021**, *11*, 1476. [[CrossRef](#)]

Disclaimer/Publisher’s Note: The statements, opinions and data contained in all publications are solely those of the individual author(s) and contributor(s) and not of MDPI and/or the editor(s). MDPI and/or the editor(s) disclaim responsibility for any injury to people or property resulting from any ideas, methods, instructions or products referred to in the content.